The influence of the probe connection on mm-wave antenna measurements

The Influence of the Probe Connection on mm-Wave Antenna Measurements

A. C. F. Reniers, A. R. van Dommele*, A. B. Smolders, *Senior Member, IEEE*, and M. H. A. J. Herben, *Senior Member, IEEE.*

Electromagnetics Group, Department of Electrical Engineering
*Mixed-signal Microelectronics Group, Department of Electrical Engineering
Eindhoven University of Technology, Eindhoven, the Netherlands
e-mail: a.reniers@tue.nl

***Abstract* — For measuring antennas in the mm-wave range commonly used connection methods like connector or probe influence the intrinsic behavior of the antenna under test. Nearby structures that support the antenna and probe or connector cause distortion on the measured antenna pattern. By comparing several simulation models of the antenna and its environment insight was obtained that helped to find a solution to reduce or avoid distortions. In order to compare with the simulations, the antenna measurements are performed with the in-house designed mm-wave anechoic chamber. Finally, there will be illustrated that the probe radiates significantly due to the discontinuity from the transitions of the probe tip to the microstrip line. This radiation influences the signal to noise ratio i.e. the dynamic range. Based on the outcome some measures that can be taken to be able to reduce this interference will be proposed i.e. improve the signal to noise ratio with approx. 15 dB.**

Keywords: Anechoic chamber, mm-wave, 60 GHz, antenna pattern measurements, LCP, antenna simulation, CST, microwave probe model, probe radiation.

I. INTRODUCTION

The interest of new wireless solutions in mm-wave frequencies is currently focused on the 60 GHz band because of the available unlicensed large bandwidth [1]. During the last few years suited antenna designs for different applications in the mm-wave range have been studied. Examples are the rod antenna [2], planar conformal antennas [3], the integration of the antenna on-chip [4] or in package [5] and deflectors [6]. Due to the small size of an individual antenna element, accurate characterization of the antenna is one of the key issues at this moment. Accurate measurement of individual antenna patterns is, for example, very important for the calibration of low side-lobe phased arrays [7]. Main challenges are: mounting the antenna under test (AUT) on a carrier, accurate alignment with respect to the reference antenna and setting up a connection with a vector network analyzer (VNA). Very often the measurement results differ from the simulation results where the differences are not fully understood. Understanding and solving these discrepancies between measurement and simulation is the main goal of this article.

In the last decade several self-designed mm-wave antenna measurement systems have been proposed. Examples are the mm-wave radiation pattern measurement setup described in [8] and mm-wave bipolar near field scanner in [9]. These papers show that there is a need for small measurement chambers with the possibility to establish a reliable connection with the AUT - without disturbing the intrinsic behavior of the antenna - and measure the reflection coefficient, gain and radiation patterns. Following these papers we designed a measurement system with a Faraday cage covered with absorbers which was used during this research. In this paper a detailed analysis of disruptive radiation from the probe body is presented. Based on this a novel probe configuration is proposed that provides radiation patterns in the 60 GHz band which closely match with simulations.

In section II, the mm-wave anechoic chamber with a modular setup will be briefly described. We will show how this anechoic environment helped us to investigate, understand and cope with the distorting influences. In section III, the AUT that is used for this research is described. Next, in section IV, two main interconnections concepts (connector and probe) will be investigated. In section V the probe radiation and the effect of nearby supporting structures will be visualized and the effects on the measured patterns illustrated and compared with simulations. In section VI, a new probe connection setup is introduced and experimentally validated.

II. THE MOBILE MM-WAVE ANECHOIC CHAMBER

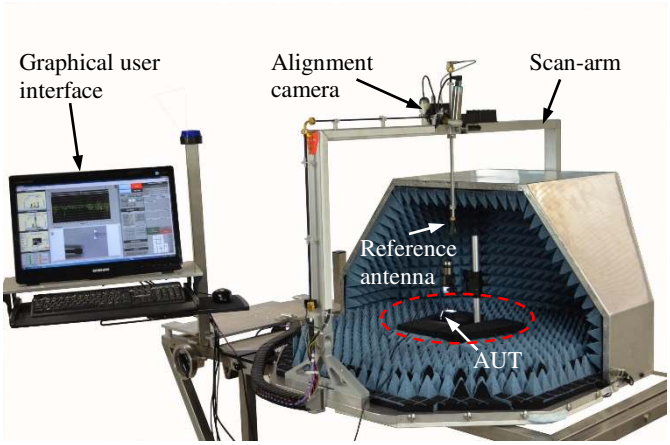

Figure 1. The mm-Wave anechoic chamber without half of its cover for illustration purposes.

The mm-wave anechoic chamber shown in Fig. 1 was designed and built for measuring new antenna concepts in the mm-wave range up to 67 GHz. The room has a diameter of 1 meter corresponding to approx. 200 wavelengths at 60 GHz.

The chamber is compact and mobile in order to be able to use it at different project-related locations. The 'central area' (red ellipse) is where the AUT is located. A close up of this area is shown in Fig. 2, where the 'probe station' and AUT itself are placed on the 'alignment table'.

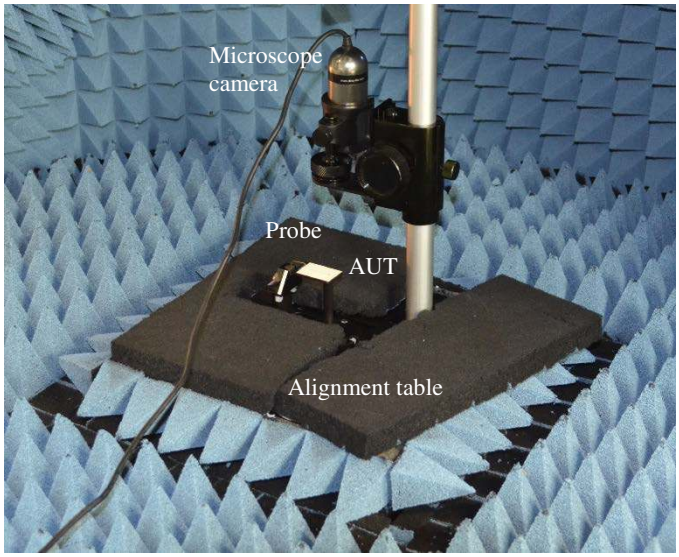

Figure 2. The setup to connect the antenna under test to the vector network analyzer with the aid of a probe.

The fully automated measurement system is controlled by nine motors for establishing a connection between probe and AUT (see Fig. 3), alignment of the AUT with respect to the reference antenna (Fig. 4), rotation of the reference antenna for choosing between Co- or Cross polarization, and for performing a variety of antenna measurements sequentially. The setup is a Faraday cage covered with absorbers to minimize environmental effects. Therefore, time-gating can be avoided. Both the connector and probe can be used within the setup, where the probe is supported and positioned with the 'probe station' shown in Fig. 3 (a) and microscope camera supporting the placement of the probe, see Fig. 3 (b).

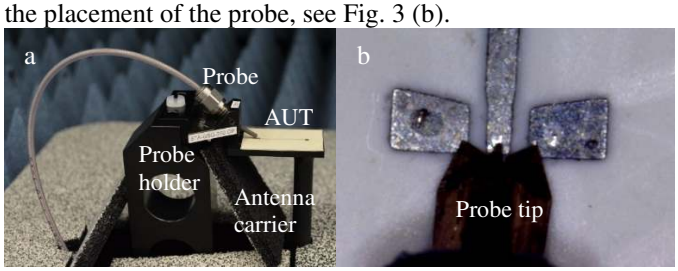

Figure 3. a) The antenna carrier, probe holder and probe and b) the view of the microscope camera supporting the placement of the probe.

The alignment is performed with the aid of the 'alignment table' shown in Fig. 4 a) and the 'alignment camera' supporting the alignment, were the view is shown in Fig. 4 (b).

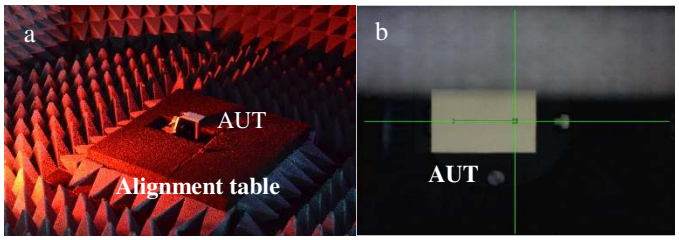

Figure 4. a) The alignment table with the AUT and probe station in the middle, and b) the support of the alignment camera to align the AUT with respect to the reference antenna.

The procedure of probe placement and antenna alignment reinsures the reproducibility of the measurement results.

III. THE INSET-FED PATCH ANTENNA

To be able to analyze the effects of the interconnection and the environment, an inset-fed patch antenna [10] mounted on a flexible substrate of liquid crystalline polymer (LCP) is used as shown in Fig. 5 (a). The pad configuration with the probe connected to the antenna is a conductor-backed coplanar waveguide (CBCPW) connected to a 50 Ohm microstrip line as shown in Fig. 5(b). The flexible substrate is mechanically supported by a specific designed 'antenna carrier' made from Polyoxymethylene (POM-C) as shown in Fig. 3 (a). The AUT is fixed on the 'antenna carrier' with the aid of vacuum. We selected this antenna because of its relative wide antenna beam, which makes it an ideal AUT to investigate the effects of the test environment and the probe.

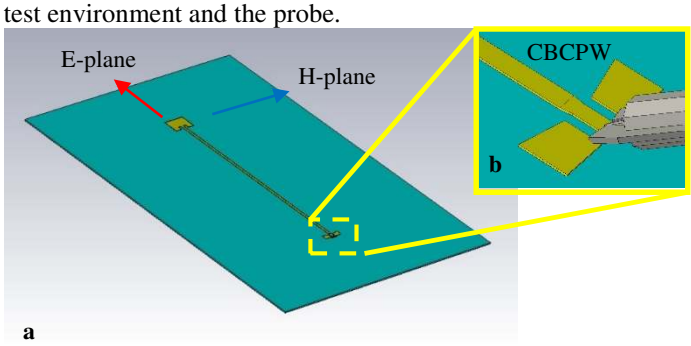

Figure 5. Simulation model of the inset-fed patch antenna.

This antenna was simulated with the finite integration technique (FIT) solver of CST Microwave Studio [11]. The resonant frequency of the AUT is 62.5 GHz and the gain is 4.7 dBi. The simulation results of both the E- and H-plane radiation patterns are shown in Fig. 6. Noteworthy is the shape of the radiation pattern in the E-plane which shows a periodical ripple caused by diffraction from the edges of the printed circuit board (PCB).

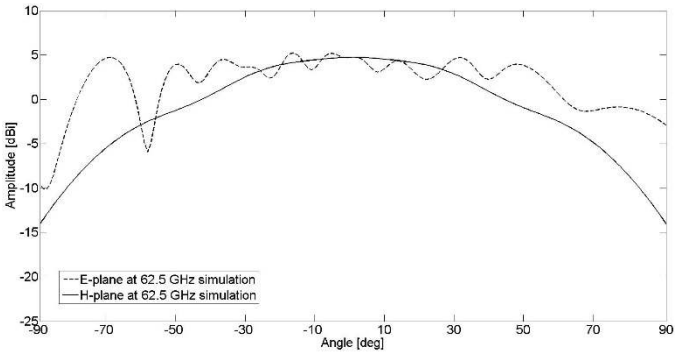

Figure 6. Simulated E- and H-plane radiation pattern at 62.5 GHz.

The CBCPW connection is designed for a ground-signal-ground (GSG) probe with a pitch of 250 µm. Already taken into account the possible reflection of the probe body, a relatively long (175 mm) microstrip line was designed to reduce possible interference. The microstrip line has a loss of approximately 1.5 dB/cm.

IV. CONNECTOR- VS PROBE-FED INTERCONNECTION

In [8], mm-wave antenna measurements with a probe are compared with connector-enabled experiments. Main conclusion is that the use of a connector introduces a larger ripple on the measured radiation pattern than the use of a probe. This is due to the fact that in [8], the connector is closer to the antenna then the probe. Therefore the reflective effects are more visible in the case of a probe. Based on this the conclusion would be that any reflective object, nearby or in line of sight should be avoided, which would be almost impossible with a connector. The advantage of a connector, however, is that it ensures a reliable and reproducible interconnection due to its rigid construction and defined position with respect to the antenna on the PCB. On the other hand, the advantage of a probe is that it results in much smaller mechanical stress on the antenna design. To ensure a reliable connection with a probe and a fair comparison between simulation and measurement it has to be placed with a certain amount of force on appropriate designed pads and on the same location where the excitation point in the simulation model is defined. Based on these findings and because of its flexibility to connect to an already existing antenna, only the probe will be used for further investigation.

There are a variety of probe models available of which the GSG probe is commonly used for unbalanced antennas. The available types vary in, for instance, probe tip pitch, extended or close-by probe tips and straight or bended probes. Also the probe body differs in size from large solid with several mounting holes to short and narrow with one mounting hole. The S-parameters of the probes are available in datasheets including the calibration coefficients. We compared two models namely the Picoprobe type 67A-GSG-250-DP probe (see Fig. 14) for the 'classical' configuration and the Picoprobe 67A-GSG-250-RVP probe (see Fig. 17) for the 'new' configuration, both types are provided by GGB Industries [12].

V. SIMULATION MODEL VERSUS MEASUREMENT SETUP

In [10], the differences between simulation and measurement have been investigated. Next to production tolerances, the significant differences are caused by the measurement set-up. Therefore we extended the antenna model with the actual probe model shown in Fig. 7 which is based on the close-by environment of the AUT in the actual measurement setup shown in Fig. 2. Interfering sources are radiation from the probe tip and obstruction and reflection from the probe body. In addition, we expect disruptive radiation from the antenna carrier which is made of POM-C and caused the waves to be diffracted at the edges of the PCB as mentioned earlier.

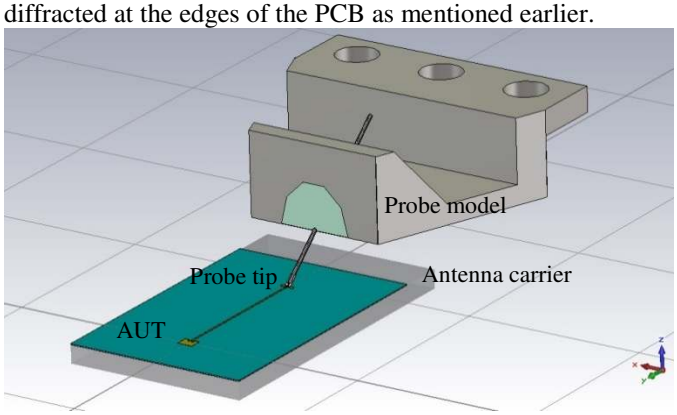

Figure 7. The simulation setup with the nearby objects.

A. *The effects of probe radiation*

In [12] it has been stated that the parasitic radiation of the probe tip limits the dynamic range of the radiation pattern:

$$SNIR_{dB} = 10\log_{10}\frac{S}{N+I} \quad (1)$$

Where S is the power of the wanted signal, N the noise power and I the total power from the interfering sources. In order to investigate this possible interference, the GSG probe model shown in Fig. 7 was connected to parallel lumped elements, representing the antenna impedance at 62.5 GHz. The resulting patterns are shown in Fig. 8. To investigate the frequency dependence of the radiation from the probe tip we determined the maximum gain of the probe radiation as function of frequency within the bandwidth of the antenna. In our simulations we adapted the impedance of the lumped element according to the expected antenna impedance for that specific frequency. It is noted that due to the ripple of the radiation pattern of the probe tip this maximum occurs for each frequency at a different angle. The variation of this maximum gain appeared to be approximately 0.5 dB over the frequency range from 50 GHz to 67 GHz. It can be concluded that for the AUT the dynamic range is approximately 25 dB. This could limit the possible radiation pattern measurement for very low gain antennas because the power at a certain angle would drop below the probe radiation level.

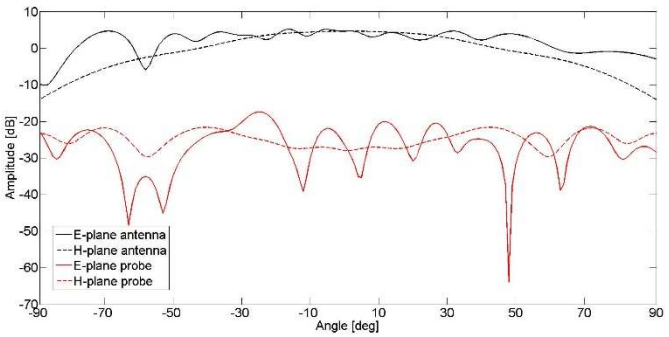

Figure 8. Simulated E- and H-plane radiation patterns of the probe versus the radiation pattern of the antenna at 62.5 GHz

To validate the simulated probe radiation we measured the AUT according to the set-up of Fig.7. Three measurements were performed to visualize the probe radiation. First the probe was positioned on the load as shown in Fig. 9 (a). Next, the AUT was connected as shown in Fig. 9 (b). Finally, the noise floor of the VNA was measured. Because the noise floor of the system does not change during a radiation pattern measurement, the noise was also measured during a 180 degree radiation pattern measurement. The measured results for both E- and H-plane and noise are shown in Fig. 10.

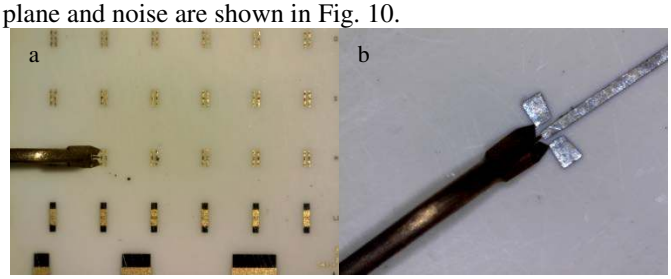

Figure 9. (a) The probe landed on the defined load and, (b) the probe positioned towards a defined load on a calibration substrate.

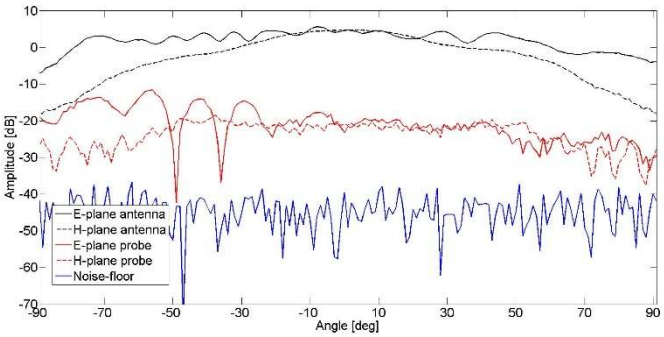

Figure 10. The E- and H-plane radiation pattern measurements of the probe (red line) versus the antenna at 62.5 GHz (black line). The noise floor (blue line) is represented with respect to the scan time.

Fig. 10 shows that the probe radiation (red line) is considerable and eliminating this interference would improve the system SNR with approx. 15 dB at 62.5 GHz. From this experiment, it can be concluded that for our AUT the probe tip radiation limits the dynamic range of the radiation pattern measurement. It does not affect the radiation pattern because it is just above the probe radiation i.e. interference level. To reduce or eliminate probe radiation an option would be to probe the antenna from the back, but to accomplish this a reliable transition through the PCB should be investigated. Another option is to design a proper transition from probe tip to the transmission line (TL) feeding the antenna which would require a study on itself.

B. The simulated effects of the close-by objects

To be able to analyze the disruptive effects on the radiation pattern in more detail, four models have been simulated, namely: (a) the ideal antenna setup, (b) the antenna with antenna carrier, (c) the antenna with antenna carrier and probe tip and (d) the complete setup including the probe body. The electromagnetic power density to illustrate the disruptive effects are shown in Fig. 11 and the corresponding E- and H-plane radiation patterns are illustrated in Fig. 12 and Fig. 13, respectively.

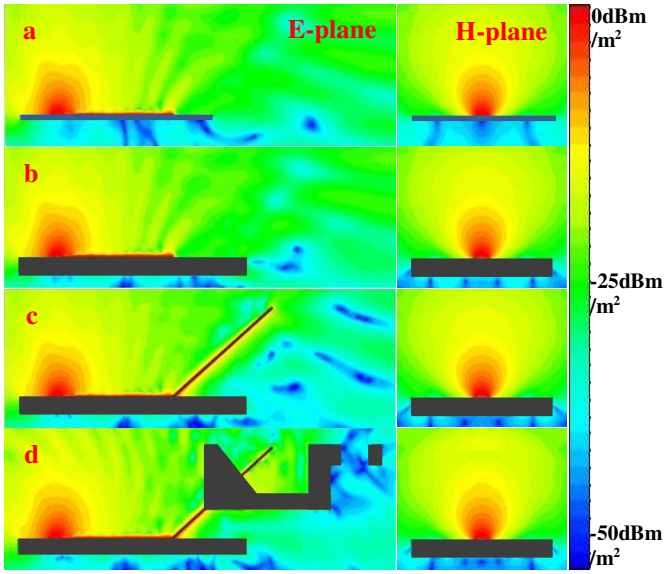

Figure 11. Simulated radiated power density [dBm/m^2] in the near-field of the antenna (side view). a) Ideal antenna, b) with carrier, c) with probe tip and the d) complete setup including the probe body. Frequency is 62.5 GHz.

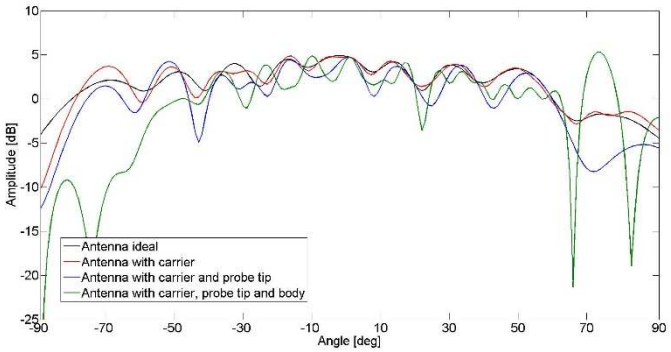

Figure 12. The simulated disturbance of the E-plane far-field radiation pattern in the four different configurations, Frequency is 62.5 GHz.

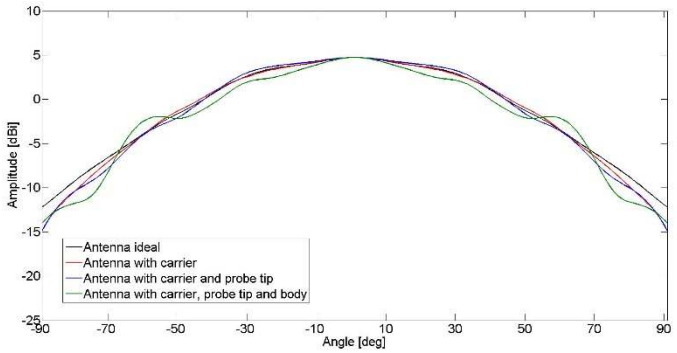

Figure 13. The simulated disturbance of the H-plane far-field radiation pattern in the four different configurations, Frequency is 62.5 GHz.

The dominant disturbing effects of the probe can easily be identified from the simulated field distribution. In Fig. 11 (c) and (d) the effect in the E-plane is visible caused by the probe tip and probe body. In addition, a small effect is visible in the H-plane caused by the 'antenna carrier', shown in Fig. 11 (a) and 11 (b). The effect of the near-field disturbances on the E-plane patterns is shown in Fig. 12. From this, we can observe small differences between the simulation models (a)-(c), but for simulation model (d), the entire pattern is strongly affected. The large pattern fluctuations between 65^0 and 90^0 are due to constructive and destructive interference from the probe body. The attenuated signal level (green line) from -90^0 to -50^0 is due to the obstruction (shadow effect) of the probe body. For the H-plane (Fig. 13), the patterns of simulation model (a)-(c) differ slightly for angles larger than 70^0 and smaller than -70^0. This is mainly caused by the antenna carrier influencing the waves diffracted from the edge of the PCB. Also in this plane the major effect is due to the probe body.

C. The measured effects of close-by objects

An Agilent E8361A (VNA) was used to perform all measurements during this research. The reference antenna placed on the scanning arm is a standard gain horn with a gain of 21 dBi at 62.5 GHz which is accurately aligned with respect to the AUT. For the measurement, the distance between the AUT and the reference antenna that satisfies the far-field criteria is generally determined by the antenna with the highest gain. That is in this case the reference antenna (21 dBi), resulting in a far-field distance of approximately 22 cm. However, the actual far field is determined at 36 cm. After analyzing this antenna structure it became clear that due to the radiation from the edges we need to take the whole antenna structure into account by determine the far field. To be able to compare and evaluate these patterns we changed the settings in our simulation environment so that it corresponds with the actual situation.

The measured and simulated patterns for the probe configuration illustrated in Fig. 14 are shown in Fig. 15 and Fig. 16, respectively. It is clear that in both cases the measurements at 22 cm disagree with the simulations without probe and antenna carrier, but agree reasonable well with the simulation of the whole setup including the probe and antenna carrier.

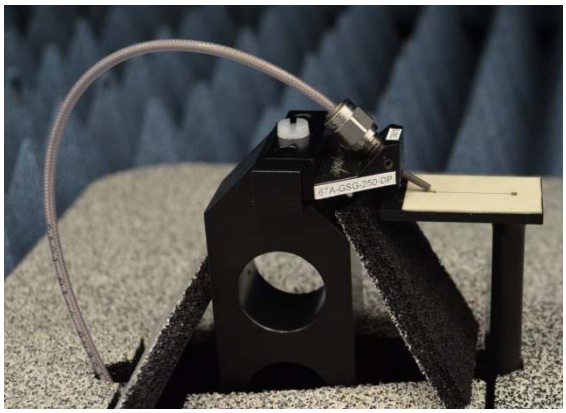

Figure 14. The 'top (classical)' probing configuration.

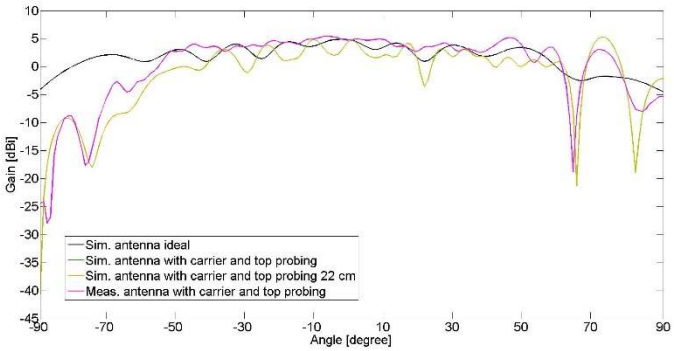

Figure 15. Radiation pattern in E-plane at 62.5GHz for 'top (classical)' probing. Measurements versus simulations.

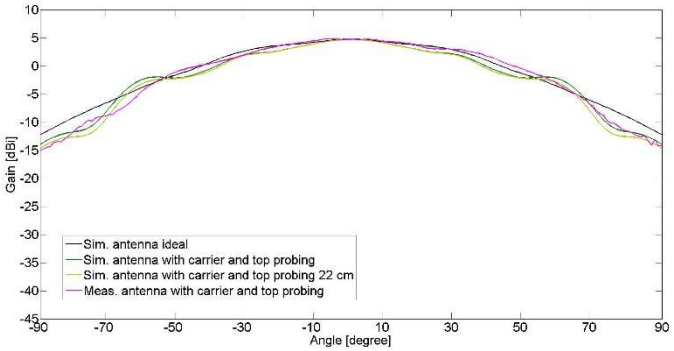

Figure 16. Radiation pattern in H-plane at 62.5GHz for 'top (classical)' probing. Measurements versus simulation.

To conclude, as expected, the probe body has the strongest effect on the measurement results. In order to improve this, we need to investigate alternative probe configurations.

VI. THE NEW PROBE SETUP AND RESULTS

In order to reduce the effect of the probe body, the setup was modified to support a probe with an alternative feed construction, as shown in Fig. 17. Also in this case the probe was implemented in the simulation model for which the results are shown in Fig. 18. The measured and simulated radiation patterns for this improved measurement setup are shown in Fig. 19 and Fig. 20.

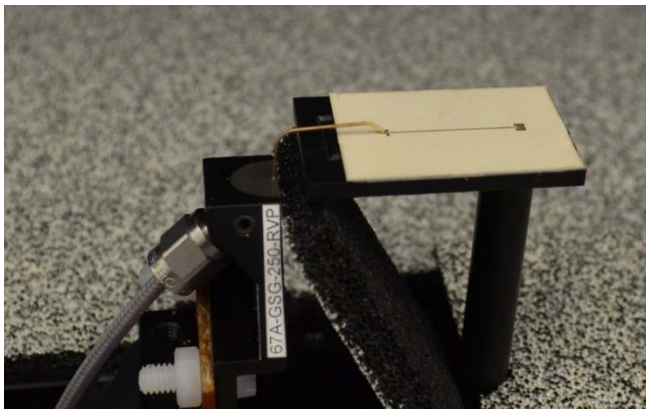

Figure 17. a) View of the '(new) Top' probing configuration. b) Probe landed on the edge of the CBCPW of the antenna.

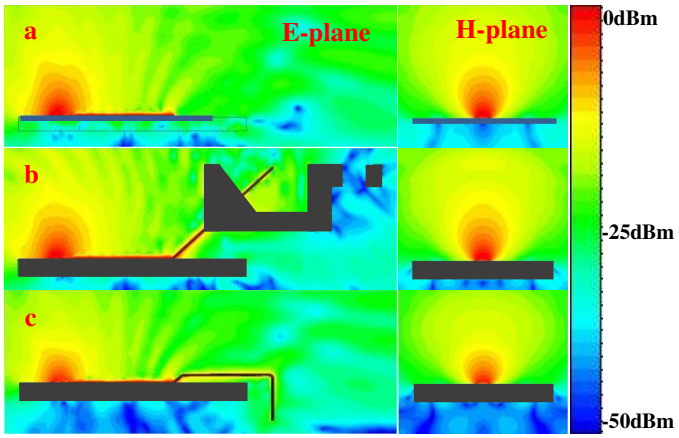

Figure 18. Simulated radiated power density [dBm/m^2] in the near-field of the antenna (side view). a) Ideal antenna, b) complete setup including the top probe body, and c) complete setup with new probe. Frequency is 62.5 GHz.

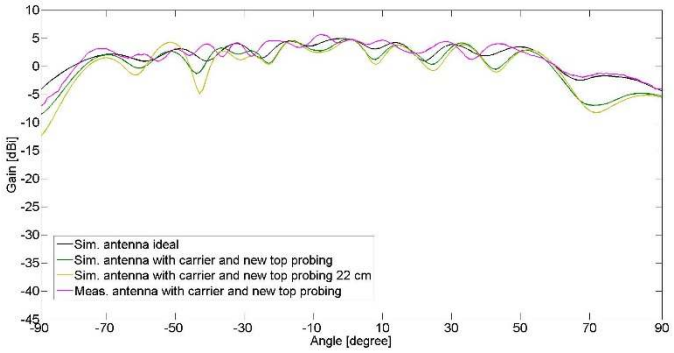

Figure 19. Radiation pattern in E-plane at 62.5GHz for '(new) top' probing. Measurements versus simulation.

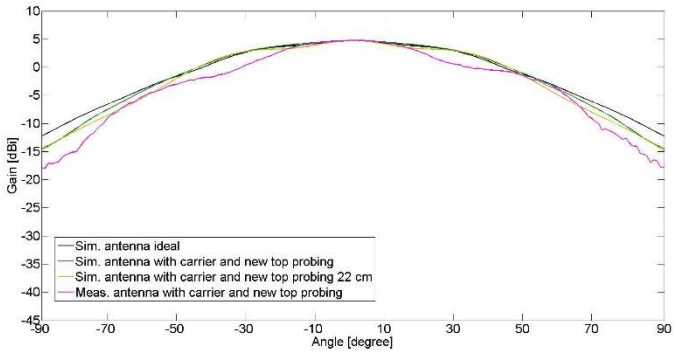

Figure 20. Radiation pattern in H-plane at 62.5GHz for '(new) top' probing. Measurements versus simulation.

Clearly, the effect of the probe-body is reduced significantly. Neither diffraction nor reflection is visible in both the E- and H-plane. The near-field distribution with the new probe configuration is shown in Fig. 18. It confirms the strongly reduced disturbance.

VII. Conclusions

It is shown that the use of a standard microwave probe for mm-wave antenna pattern measurements seriously deteriorates the measurement accuracy. The probe body causes blockage and reflections and the probe-tip generates unwanted radiation. It limits the dynamic range of the setup to approx. 15 dB and will affect the radiation pattern measurement for low gain (< 0 dBi) antennas.

In a step-by-step approach we have shown that the probe body is the main problem. Therefore, we have introduced an alternative probe configuration with a bended extended tip in a new designed setup.

Overall the disturbing effects of the bended probe on the radiation pattern measurement of our highly sensitive patch antenna are so small that the measured results agree very well with the simulated antenna pattern.

References

[1] WiGig Alliance (2010), Defining the future of multi-gigabit wireless communications. WiGig White paper. http://www.wirelessgigabitalliance.org/ ?getfile=1510

[2] Rousstia, M.W. & Herben, M.H.A.J. (2013). High performance 60-GHz dielectric rod antenna with dual circular polarization. Proceedings of the European Microwave Week, Nuremberg, Germany, 6-11 October 2013, 1-4.

[3] Huang, M.D., Herben, M.H.A.J. & Kazim, M.I. (2011). Design of cylindrically bent antenna array on LCP substrate with large coverage at 60 GHz. Proceedings of the 5th European Conference on Antennas and Propagation (EUCAP), 11-15 April 2011, 1117-1121.

[4] Johanssen, U, A.B. Smolders, R. Mahmoudi, I. Akkermans, "Substrate Loss Reduction in Antenna-on-Chip Design", Proc. of the IEEE AP-Symposium 2009, pp. 1-4 , June 2009.

[5] U. Pfeiffer, J. Grzyb, D. Liu, B. Gaucher, T. Beukema, B. Floyd, and S. Reynolds, "A chip-scale packaging technology for 60- GHz wireless chipsets," IEEE Transactions on Microwave Theory and Techniques, vol. 54, no. 8, pp. 3387 –3397, aug. 2006.

[6] Kazim, M.I. & Herben, M.H.A.J. (2011). Trade-offs in multifaceted passive electromagnetic deflector for the 60 GHz frequency band. Proceedings of the 5th European Conference on Antennas and Propagation (EUCAP), Rome, Italy, 11-15 April 2011, 1044-1048.

[7] Smolders A.B. and G.A. Hampson, “A fast and accurate scheme for calibration of active phassed-array antennas”, Proceedings IEEE Antennas & Propagation Symposium Orlando, pp 1040-1043, 1999.

[8] Titz D., Ferrero F., Luxey C. & Jacquemod G. (2011). A novel fully-automatic 3D radiation pattern measurement setup for 60 GHz probe-fed antennas. Proceedings IEEE International Symposium on Antennas and Propagation (APSURSI), 3-8 July 2011, Spokane, Washington, U.S.A., 3121– 3124.

[9] Brockett, T. ; Rahmat-Samii, Y. A. (2008). Novel portable bipolar near-field measurement system for millimeter-wave antennas: construction, development, and verification. Antennas and Propagation Magazine, IEEE. Volume: 50 , Issue: 5. Page(s): 121 – 130.

[10] Huang, M.D. ; Herben, M.H.A.J. ; Reniers, A.C.F. ; Smulders, P.F.M. (2013). Causes of discrepancies between measurements and em simulations of millimeter-wave antennas. Antennas and Propagation Magazine, IEEE. Volume: 55 , Issue: 6. Page(s): 139 – 149.

[11] MicroWave Studio. www.cst.com

[12] GGB Industries Inc. Picoprobe. www.ggb.com.

[13] Mohammadpour-Aghdam, K., Brebels, S., Enayati, A., Faraji-Dana, R., Vandenbosch, G.A.E. & DeRaedt, W (2011). RF probe influence study in millimeter-wave antenna pattern measurements. International Journal of RF and Microwave Computer Aided Engineering, 21(4) 413-420.

.